International Journal of Mechanical, Industrial and Aerospace Sciences
ISSN: 2517-9950
Vol:7, No:4, 2013

Experimental and Numerical Study of the Effect of Lateral Wind on the Feeder Airship

A. Suñol, D. Vucinic, S.Vanlanduit, T. Markova, A. Aksenov, and I. Moskalyov

***Abstract*—**Feeder is one of the airships of the Multibody Advanced Airship for Transport (MAAT) system, under development within the EU FP7 project. MAAT is based on a modular concept composed of two different parts that have the possibility to join; respectively they are the so-called Cruiser and Feeder, designed on the lighter than air principle. Feeder, also named ATEN (Airship Transport Elevator Network), is the smaller one which joins the bigger one, Cruiser, also named PTAH (Photovoltaic modular Transport Airship for High altitude),envisaged to happen at 15km altitude.

During the MAAT design phase, the aerodynamic studies of the both airships and their interactions are analyzed. The objective of these studies is to understand the aerodynamic behavior of all the preselected configurations, as an important element in the overall MAAT system design. The most of these configurations are only simulated by CFD, while the most feasible one is experimentally analyzed in order to validate and thrust the CFD predictions. This paper presents the numerical and experimental investigation of the Feeder "conical like" shape configuration. The experiments are focused on the aerodynamic force coefficients and the pressure distribution over the Feeder outer surface, while the numerical simulation cover also the analysis of the velocity and pressure distribution. Finally, the wind tunnel experiment is compared with its CFD model in order to validate such specific simulations with respective experiments and to better understand the difference between the wind tunnel and in-flight circumstances.

***Keywords*—**MAAT project Feeder, CFD simulations, wind tunnel experiments, lateral wind influence.

I. Introduction

THE Feeder airship is part of the MAAT system [1]-[2]. The ATEN feeders perform linking operations between cruisers and ground based airport hubs. They are designed to lift up and down, from the ground to the interception altitude, where they join the PTAH to form a unique system. The PTAH remains in flight at an economical altitude and proper speed, and it has static hovering capabilities to enable the ATEN feeder docking operations. This economical altitude is defined to be between 13 and 15 km. Fig. 1 illustrates the MAAT system concept, in continuous development.

A. Suñol is with the Vrije Universiteit Brussel, Brussels 1050, Belgium. (e-mail: anna.sunol.jimenez@vub.ac.be).
D. Vucinic is with the Vrije Universiteit Brussel, Brussels 1050, Belgium (e-mail: dean.vucinic@vub.ac.be).
S. Vanlanduit is with the Vrije Universiteit Brussel, Brussels 1050, Belgium (e-mail: svlandui@vub.ac.be).
T.Markova, is with Tesis, Moscow, Russia. (e-mail: markova@flowvision.ru).
A. Aksenov is with Tesis, Moscow, Russia. (e-mail: andrey@tesis.com.ru).
I. Moskalyovis with Tesis, Moscow, Russia. (e-mail: miv@flowvision.ru).

The aerodynamic analysis presented in this paper, is focused on one selected Feeder configuration, which has the particular conical shape, as shown in Fig. 2, designed by the University of Modena and Reggio Emilia (UNIMORE) [1], being the MAAT project leader. The main movement of the Feeder is vertical- like an elevator -since it interconnects the Cruiser and the ground airport hub. This vertical movement is performed by the Feeder variable volume characteristics, based on the buoyancy principle, enabling its up and down movement. However, the Feeder is expected to face the horizontal winds during the traversed altitudes, which are often experienced as being part of the typical meteorological conditions. Moreover, Feeder must be able to move horizontally, in order to join the Cruiser. In this paper, the influence of the low-speed wind at high altitudes is studied, with special aim to estimate the aerodynamic loads and the pressure distribution during the Feeder prescribed movement. The presented results are obtained via numerical simulations [3] and wind tunnel experiments [4], and further on, validated by their comparison [5], [6]. A second CFD simulation studying the wind tunnel conditions is carried out, in order to shed light on the difference between in-flight and wind tunnel conditions. The main reason behind performing a CFD simulation of the wind tunnel experiment is due to the difference in the Reynolds number between the in-flight and wind tunnel conditions.

The experiments have been performed in the Mechanical Engineering lab at the Vrije Universiteit Brussel (VUB). The used CFD numerical simulation software is Flow Vision, by Tesis, which has been used by VUB in several EU projects [7].

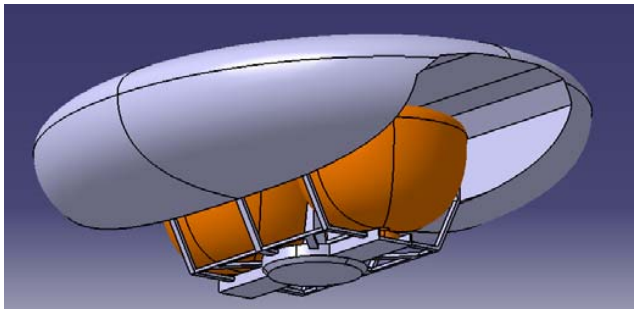

Fig. 1 MAAT system

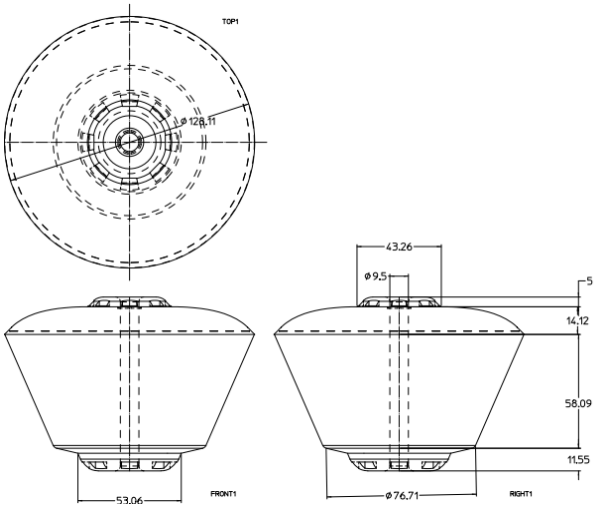

Fig. 2 Feeder geometry

II. Numerical Simulation

The influence of the low-speed wind at high altitude is simulated. The applied atmospheric parameters for the initial and boundary conditions are shown in Table I. The velocity and relative pressure (defined as difference between the pressure value at the selected point and at infinity) distributions along the symmetry plane are plotted in Fig. 3 and Fig. 4. The obtained aerodynamic coefficients are presented in Table II, while Fig. 9, Fig. 10 and Fig. 11 show the time dependent variation of the aerodynamic forces. The variation of the aerodynamic forces influences the stability of the Feeder and thus needs to be considered in details. Fig. 5 and Fig. 6 show the irregular air flow pattern due to the vortex shedding, which induces an unsteady behavior. Fig. 7 and Fig. 8 show the pressure distribution over the Feeder surface. The force coefficients are calculated applying (1), (2) and (3), where L, is the lift force, D is the drag force, M is the pitch moment, C_L, C_D and C_M are the aerodynamic force coefficients, ρ is the air density, v is the air speed, S_p is the plane surface, S_f is the frontal surface and l is the characteristic length, which is the maximum diameter of the model. As Feeder is a bluff body, the frontal surface is applied to calculate the drag coefficient [8].

$$C_L = \frac{L}{0.5\rho v^2 S_p} \tag{1}$$

$$C_D = \frac{D}{0.5\rho v^2 S_f} \tag{2}$$

$$C_M = \frac{M}{0.5\rho v^2 S_p l} \tag{3}$$

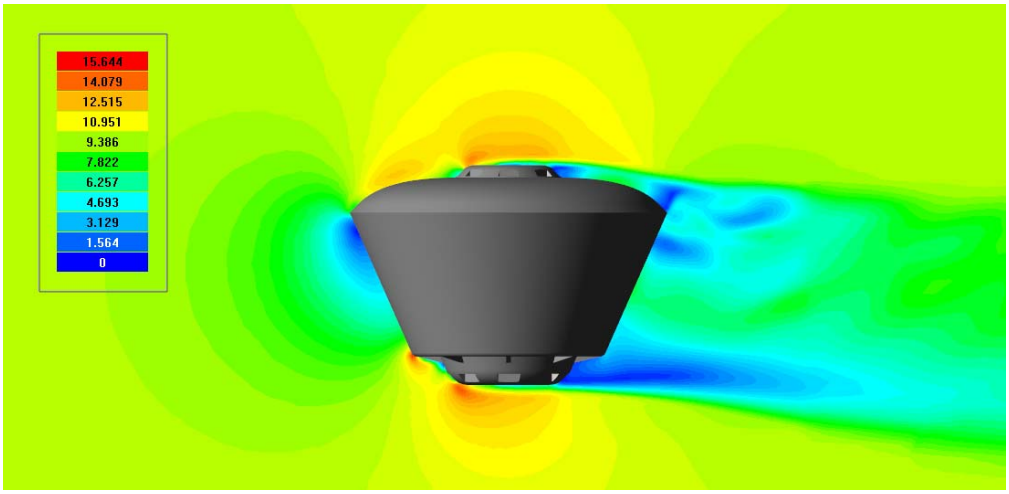

Fig. 3 Air velocity [m/s] in the plane

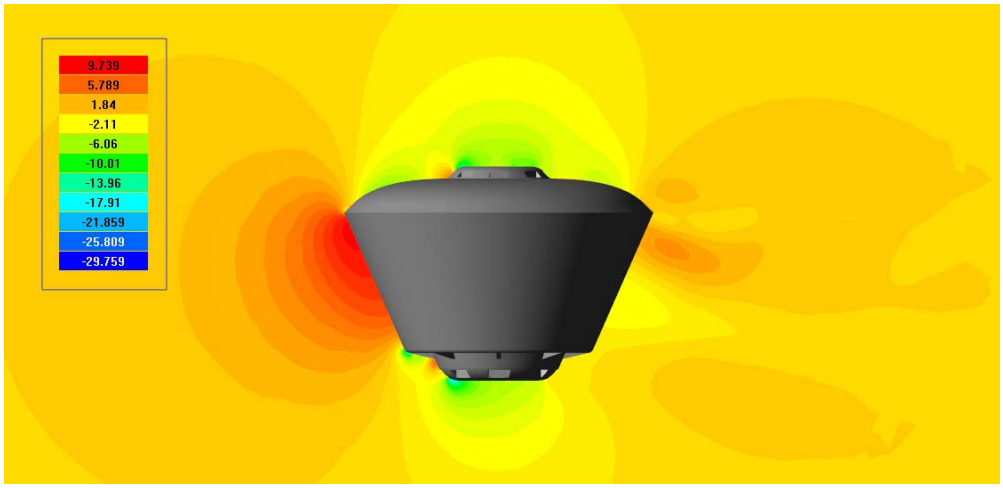

Fig. 4 Relative pressure [Pa] in plane

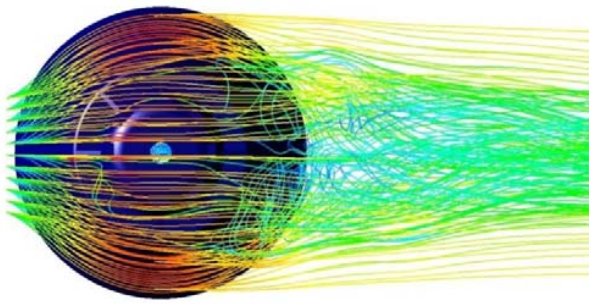

Fig. 5 Streamlines

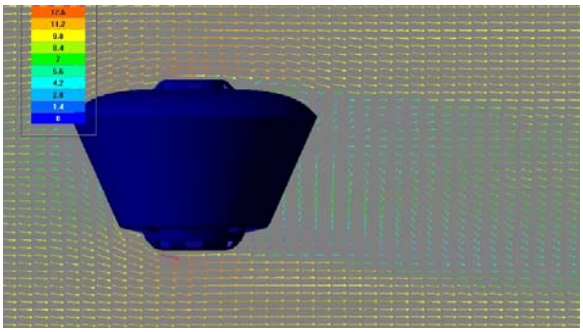

Fig. 6 Vector velocity field

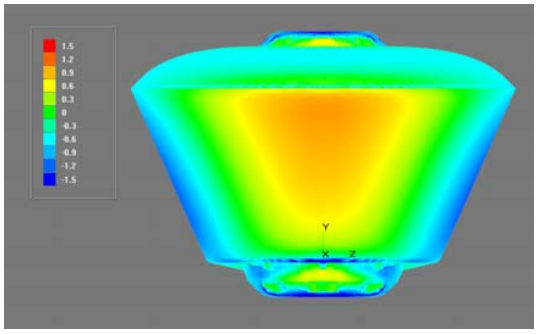

Fig. 7 Pressure distribution. Frontal view

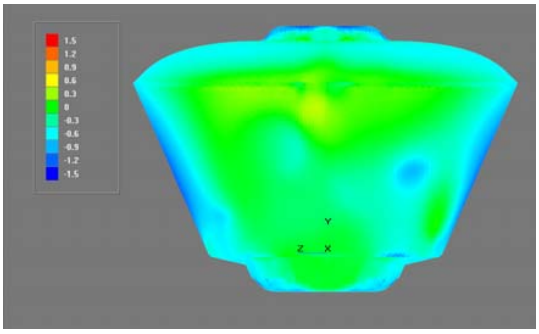

Fig. 8 Pressure distribution. Rear view

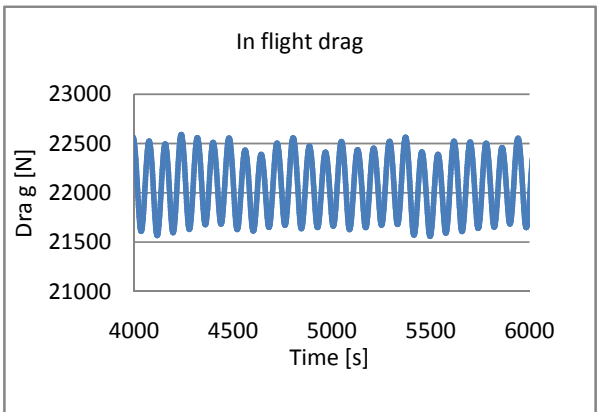

Fig. 9 Drag variation along time at 15 km altitude at constant speed of 10 m/s

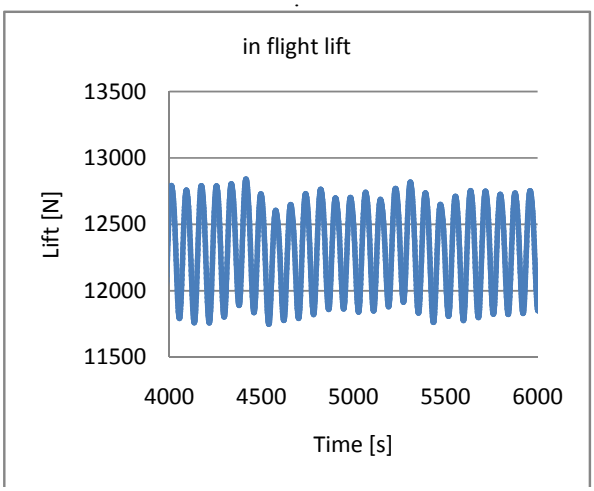

Fig. 10 Lift variation along time at 15 km altitude at constant speed of 10 m/s

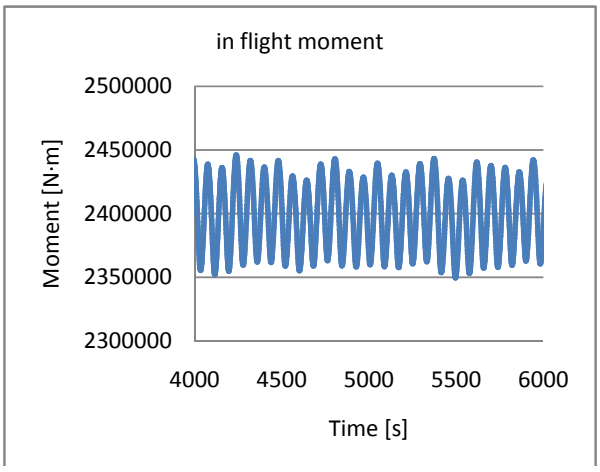

Fig. 11 Pitch moment variation along time at 15 km altitude at constant speed of 10 m/s

TABLE I
ATMOSPHERIC PARAMETERS

Altitude	15 km
Pressure, Pa	12110
Dynamic viscosity, Pa-s	1.4216e-5
Density, kg/m^3	0.19476
Speed, m/s	10

TABLE II
RESULTS OF THE INITIAL SIMULATIONS

Drag	C_d	Lift	C_l	Pitch	C_m
[kN]	[-]	[kN]	[-]	[kN·m]	[-]
22.0	0.274	12.4	0.099	2395.8	0.149

III. EXPERIMENTAL SIMULATION

The wind tunnel in which the experiments have been performed is of the Eiffel type. It is composed of the inlet, settling chamber, contraction cone, test section, diffuser, drive section and exhaust outlet part. The total length of the wind tunnel is 14m. The air energizing is done by blowing. In the settling chamber, several honeycombs are used to rectify the lateral and axial turbulence. The test section is closed. The maximum speed is 20 m/s, and the dimensions of the test section are 1m height per 2m width [9].

The ratio of the frontal area of the model and the wind tunnel test section should be approximately 5% in the case of bluff bodies [10]; the scale of 1:250 is applied for the experimental Feeder model.

The height of the model is 355mm and the maximum diameter is 512mm. The frontal area of the model is 0.13 m^2. A master piece of the model is manufactured by elimination of material [11], using an ICP 4030 machine. The final shell model is manufactured using composite materials. Two separable parts are created, which enables the placement of the pressure taps.

Considering the model dynamic similarity, in this low-speed wind tunnel experiment, the parameter to match is the Reynolds number. At 10m/s and 15 km height, and considering the ISA model, the resulting Reynolds number is $14.99 \cdot 10^6$. As mentioned, the maximum speed of the wind tunnel is 20 m/s, and thus the corresponding Reynolds number can not be achieved. Comparing the results at different speeds, the influence of the Reynolds number is estimated. The tested speeds are: 5, 10, 12, 14, 16 and 18 m/s.

A. Force Balance

The aerodynamic force coefficients are determined by a force balance with 6 degrees of freedom. In order to not exceed the range of the force balance due to the high drag, the model is also connected to the ceiling of the wind tunnel. The gravity center of the model (located at 202 mm from the

model bottom) is placed in the mid-section of the wind tunnel, as shown in Fig. 12 and Fig. 13. As the upper support disturbs the lift force recorded by the force balance, an additional experiment just with the lower support is performed. In this case, only speeds up to 12 m/s are tested. The sampling frequency is 1 kHz, and the number of samples is 1000.

During the experiment, the reactions on the force balance and the flow properties are recorded. The reactions in the ceiling are considered to be of the same value at the wind tunnel floor, due to symmetry, as shown in (4), (5) and (6), where F_x, F_z and M_y are the reactions measured by the force balance in the respective axis directions; D, L and M are the aerodynamic forces and pitch moment; $d_{FB-model}$ is the distance between the gravity center of the model and the force balance. In order to study the experimental errors, the standard deviation for all the measurements is also recorded. The force coefficients are calculated as shown in (1), (2) and (3). Setting outto subtract the drag due to the presence of the support, a wind-run has been performed only with the support present. The drag of the support is divided by the dynamic pressure and the frontal surface of the model, multiplied by 2 to take into account both the upper and lower support, and subtracted to the drag coefficient obtained from the system supports-model. The errors are calculated considering the accuracy and resolution of the measurement devices and taking into account the standard deviation of the measurement data. A statistical normal distribution is assumed and the error calculation is performed, as explained in detail in [12].

$$D = 2F_x \tag{4}$$

$$L = F_z \tag{5}$$

$$M = 2M_y - D \cdot d_{FB-\mathrm{mod}el} \tag{6}$$

Fig. 12 Experimental model

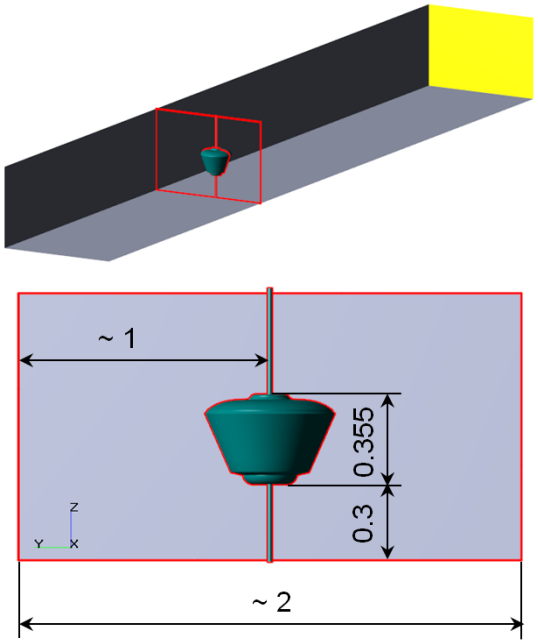

Fig. 13 Experimental set up

B. Pressure Taps

The pressure distribution is measured by the pressure taps. The position of the model and the supports used are the same as in the force balance experiment. The multi pressure transducer Scanivalve Corp. of 64 ports is connected to the holes drilled in one cross-section of the model. The wire is connected to a static port in the free-stream to record the static pressure. The model is sequentially rotated over 180º in order to study the entire surface. The sections at 0º, 22.5º, 45º, 72.5º, 90º, 111.5º, 135º, 157,5º and 180º are studied, considering 0º the section aligned to the wind direction. The same values of the pressure are considered to be symmetrically equal, thus only half of the model was tested. A frequency of 1 Hz is used, and the number of samples is 200. Eq.7 is applied to calculate the pressure coefficient at each point. Graphic results are obtained via MatLab software and shown respectively in Fig. 14 and Fig. 15. In order to validate the pressure taps and force balance experiments, the drag and lift coefficient are also calculated from the measurements data obtained from the pressure taps. The calculation is done by applying a mean pressure coefficient to the rectangular discrete surfaces, defined and delimited by the four taps locations, as shown in (8). The area of each surface element is calculated, as described in (9), to define their contributions, respectively for the drag and lift coefficients calculated by using (10) and (11).

$$c_p = \frac{p - p_\infty}{0.5\rho v^2} \tag{7}$$

$$c_{p_i} = \frac{c_{p_{nw}} + c_{p_{sw}} + c_{p_{ne}} + c_{p_{se}}}{4} \tag{8}$$

$$S_i = 2\pi \frac{22.5}{360} r_i \left| z_n - z_s \right| \tag{9}$$

$$C_L = \frac{\sum c_{p_i} \cdot \sin(\alpha_i) S_i}{S_p} \tag{10}$$

$$C_D = \frac{\sum c_{p_i} \cdot \cos(\alpha_i) S_i}{S_f} \tag{11}$$

where $p - p_\infty$ is the difference of the pressure perpendicular to the pressure tap and the static pressure of the free-stream, c_p is the pressure coefficients and subscripts nw, ne, sw and se refers to the four surface corners, S_i is each discrete surface, r_i is the main distance to the central axis of the surface, z_n is the height of the upper and z_s of the lowersurface element, and α_i is the angle between the vector perpendicular to the surface and the horizontal axis. The errors are calculated using the same procedure as applied in the force balance data analysis.

C. Experimental Results

In Table III are shown, the aerodynamic force coefficients calculated from the force balance measurements. The drag due to the support has been already subtracted, which would otherwise contribute with an additional drag coefficient of value 0.0774. The expectable error due to the measurement devices is included. In Table IV are shown the force coefficients calculated by pressure taps. In Fig. 14 and Fig. 15 the pressure distribution expressed in terms of pressure coefficient, c_p is shown.

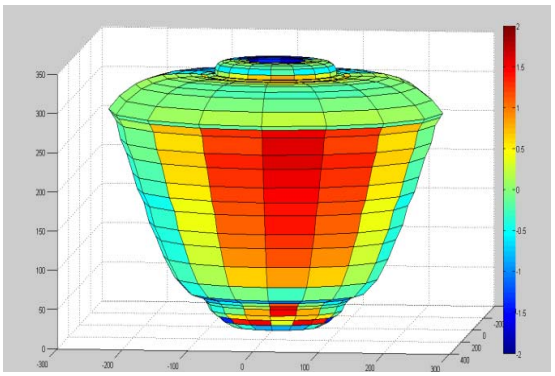

Fig. 14 High pressure zone

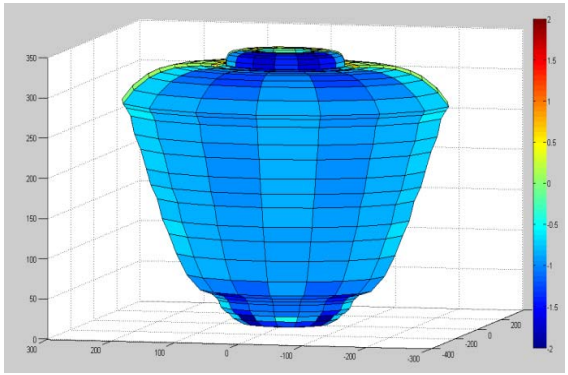

Fig. 15 Low pressure zone

TABLE III
FORCE COEFFICIENTS CALCULATED BY FORCE BALANCE

speed [m/s]	5	8	10	12	14	16	18
C_D	0,3523	0,3368	0,3331	0,3338	0,3316	0,3325	0,3270
C_D error	±0,0064	±0,0045	±0,0037	±0,0040	±0,0041	±0,0031	±0,0029
C_L	0,1769	0,1623	0,1609	0,1611	-	-	-
C_L error	±0,0067	±0,0031	±0,0023	±0,0019	-	-	-
C_M	0,2902	0,2285	0,2262	0,2269	0,2259	0,2263	0,2235
C_M error	±0,0049	±0,0027	±0,0025	±0,0027	±0,0028	±0,002+	±0,0025

TABLE IV
FORCE COEFFICIENTS CALCULATED BY PRESSURE TAPS

speed [m/s]	5	8	10	12	14	16	18
C_D	0,3090	0,3147	0,3196	0,3364	0,3351	0,3270	0,3293
C_L	0,0203	0,1416	0,1562	0,1353	0,1399	0,1522	0,1380

IV. CFD VALIDATION OF THE WIND TUNNEL EXPERIMENT

In order to shed light on the error due to the difference of the Reynolds number between in-flight and wind tunnel conditions, a numerical simulation of the experiment has been performed. In addition to the validation of the experimental results, already obtained by comparing the results coming from two different experiments, a wind tunnel CFD simulation is used as a tool to elucidate the expectable difference between the two considered cases. The oscillating character of the aerodynamic force coefficients is specially considered.

The numerical simulation input has been defined in accordance with the experiment performed at a speed of approximately 16 m/s, as shown in Table V. Velocity and pressure distributions along the symmetry plane are plotted in Fig. 16 and Fig. 17. The aerodynamic coefficients of the drag force and lift obtained via numerical simulation are presented in Table VI, while the variation with time is shown in Fig. 18 and Fig. 19.

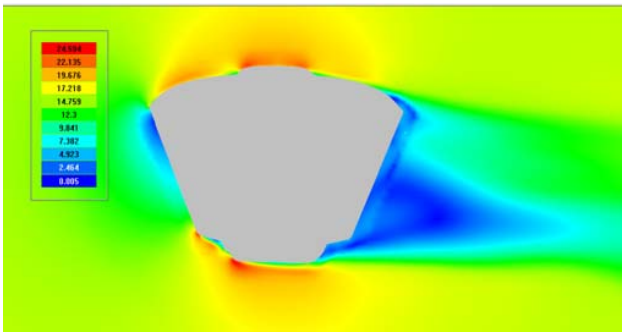

Fig. 16 Air speed [m/s] in plane

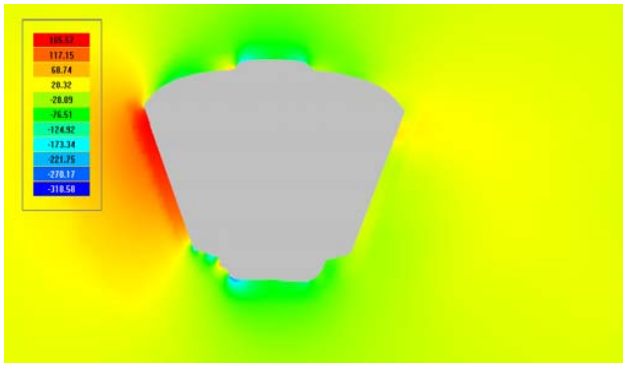

Fig. 17 Relative pressure [Pa] in plane

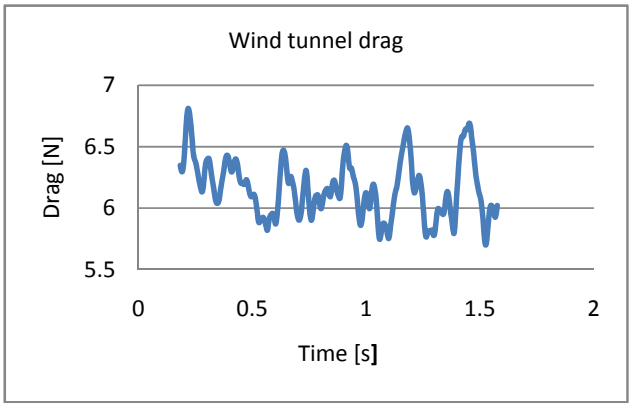

Fig. 18 Drag variation for the wind tunnel conditions

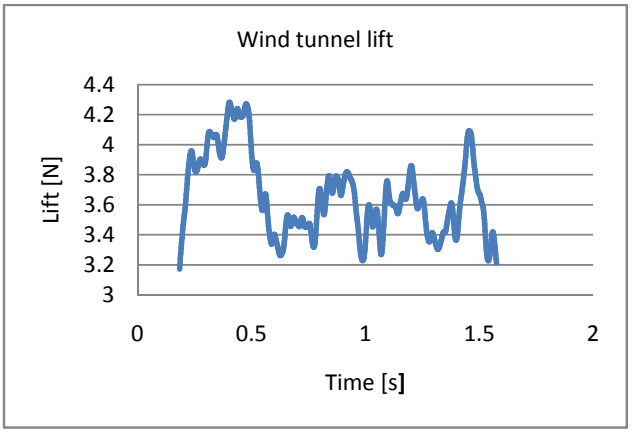

Fig. 19 Lift variation for the wind tunnel conditions

TABLE V
ATMOSPHERIC PARAMETERS

Altitude	0 km
Pressure, Pa	100476.4
Dynamic viscosity, Pa-s	1.6e-5
Density, kg/m^3	1.1689
Temperature, K	299.5
Speed, m/s	15.83

V. COMPARISON AND ANALYSIS OF THE RESULTS

As already mentioned, the Reynolds number was not matched in the performed experiment due to the maximum

speed limit of the wind tunnel. A range of speeds have been tested, and the evolution of the drag coefficient in respect to the Reynolds number is shown in Fig. 20. Considering the Feeder shape, the same type of evolution as in the case of the sphere, shown in Fig. 21[13], is found expectable. According to Fig. 21, the tested range is within the phase where the point of the boundary layer detachment is moving backwards due to the increase of the present kinetic energy. It is expectable that the drag coefficient of the prototype will be similar to the one obtained experimentally, since the detachment of the boundary layer decrease the pressure drag, while the higher level of viscosity will increase the viscous drag. The comparison of the velocity profile at both conditions, represented at Fig. 22 and Fig. 23confirms this conclusion by showing the delayed position of the detachment point in the boundary layer.

Table VI shows a comparison of all the achieved results. The difference of the drag coefficients obtained by the two CFD analyses is due to the difference in Reynolds number. Thus, the experimental drag coefficient obtained is higher than the in-flight drag coefficient. The drag coefficient obtained experimentally and computationally, considering wind tunnel conditions are found similar. On the contrary, there is a difference in the lift coefficients. The most probable reason is the absence of a vertical hole in the model, which is present in the CFD simulations. This hole connects top and bottom walls of the central section, influencing in the pressure distribution.

Regarding the instabilities present in the numerical results, the standard deviation of the drag coefficient has been studied. CFD in flight results show a steady behavior, with oscillations of just 1.14%. The oscillations are due to the unsteady pattern characteristic of the vortex shedding effect. The wind tunnel CFD shows a higher value of oscillations, due to the larger wake generated at the lower Reynolds number. The experimental results show a considerably higher level of oscillations. One possible explanation might be that the vibrations are created by a poor linkage of the support with the model.

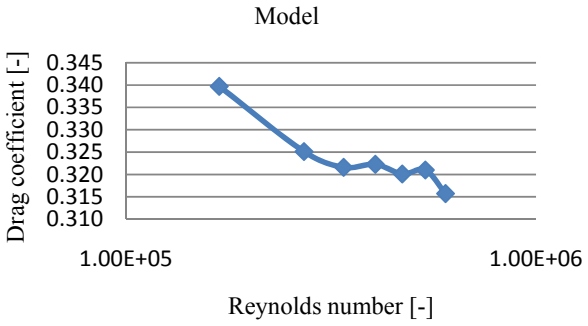

Fig. 20 Influence of Reynolds number in the drag coefficient of the model

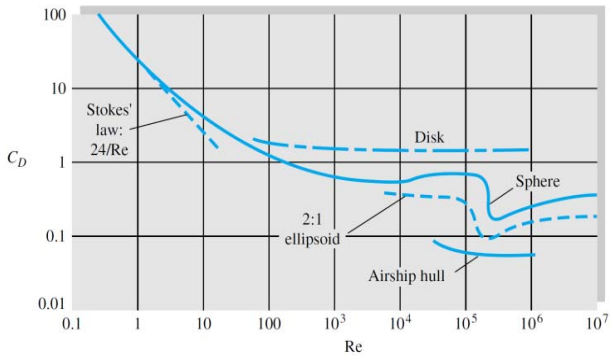

Fig. 21 Influence of Reynolds number to the drag coefficient of a sphere

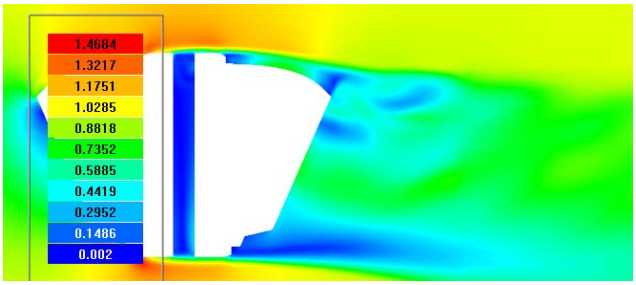

Fig. 22 Detachment of the boundary layer at in flight conditions

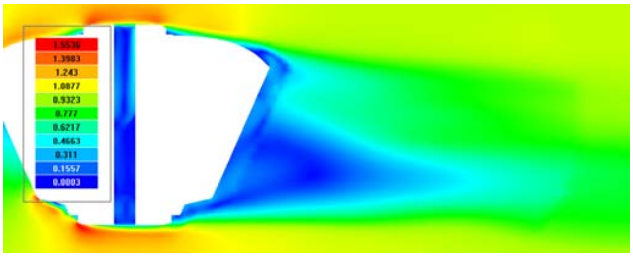

Fig. 23 Detachment of the boundary layer at wind tunnel conditions

TABLE VI
COMPARISON OF RESULTS

	C_D	C_L	%oscillations
Experimental analysis	0.327	0.161	19.43
In flight CFD	0.274	0.099	1.14
Wind tunnel CFD	0.318	0.117	2.79

VI. CONCLUSIONS

In this paper, the aerodynamic performance of the Feeder airship is simulated numerically and experimentally. The identified error between experiment and the respective CFD simulation, modeling the wind tunnel conditions, has been analyzed.

Several conclusions are extracted from the simulations:

1. The validation of the CFD results is achieved by comparing them with the respective experimental results.
2. At the low Reynolds number, theinvestigated conical Feeder configuration shows stable aerodynamic characteristics. The oscillations of the drag force are found to be quite low.
3. The aerodynamic performance of the conical shaped Feeder depends highly on the Reynolds number.
4. The presented numerical simulation approachis found appropriate to deal with the experimental limitations. For the presented test case, as it is not possible to reach the equivalent Reynolds number, a complementary CFD study is carried out to explainthe encountered differences.
5. The results obtained are similar to the already reported aerodynamic analysis within the MAAT consortium, which only performed CFD, as presented in [3].

It is expected that a similar study will follow up in respect to the Feeder-Cruiser interaction model, with the objective to develop the base modeling approach for the docking and joint operations, which represents the crucial MAAT development challenge, which has to be solved in order to come up with the complete and viable design of the envisaged MAAT system.

ACKNOWLEDGMENTS

The presented work in this paper was performed as part of the Multibody Advanced Airship for Transport (MAAT) project with ref. 285602, supported by European Commission through the 7th Framework Programme, and which is gratefully acknowledged.

We would like to acknowledge the data provided by the MAAT partner, the University of Hertfordshire Higher Education Corp. (UH), whose results have been considered as guidance during the performed experimental and numerical analysis.

REFERENCES

[1] "MAAT project website," 2012. [Online]. Available: http://www.eumaat.info.
[2] M. Trancossi, A. Dumas, M. Madonia, J. Pascoa and D. Vučinić, "Fire-safe Airship System Design," SAE International Journal of Aerospace, no. 5:11-21; doi:10.4271/2012-01-1512, 2012.
[3] V. Pshikhopov, M. Medvedev, M. Neydorf, R. Krukhmalev, V. Kostjukov, A. Gaiduk and V. Voloshin, "Impact of the Feeder Aerodynamics Characterisctics on the Power of Control Actions in Steady and Transient Regimes," SAE , 2012.
[4] D.Vučinić, B.K.Hazarika and C.Dinescu, "Visualization and PIV Measurements of the Axisymmectric In-Cylinder Flows," in ATT Congress and Exhibition, Barcelona, 2001.
[5] D. Vučinić and B. K. Hazarika, "Integrated Approach to Computational and Experimental Flow Visualization of a Double Annular Confined Jet," Journal of Visualization, Vols. Vol.4, No. 3, 2001.
[6] D. Vučinić, A. D. Mets, S. van der Elst, B. Van Der Heggen, K. Nuyten and R. d'Ippolito, "3D-TestBench – collaborative 3D engineering framework integrating workflows and knowledge-based tools," in NAFEMS World Congress 2011, Boston, USA, 2011.
[7] A. Aksenov, D. Korenev, A. Shyshaeva, Z. Mravak and D. Vučinić, ""Drop-Test" FSI simulation with Abaqus and FlowVision based on the direct 2-way coupling approach," in Abaqus Users, Newport, Rhode Island, USA, 2007.
[8] F. M.White, Fluid Mechanicsp.413-414, Mc. GrawHill, 2008.
[9] A. Suñol, Experimental aerodynamic study of Airship Transport Elevator Network, Msc. Thesis. Vrije Universiteit Brussel, 2012.
[10] Barlow J.B., Rae W.H and Pope A., Low-speed wind tunnel testing, 3rd edition, p.65, John Wiley & Sons, 1999.
[11] D.T.Pham and R.S. Gault, "A comparison of rapid prototyping technologies," International Journal of machine tools and manufacture, no. 38, 1998.
[12] B. Barlow, William H. Rae and Alan Pope, Low speed wind tunnel testing,3rd edition, pp.445-457, John Wiley & Sons, 1999.
[13] F. M. White, «Fluid Mechanics,» p.417, Mc. GrawHill, 2008.